MNRAS **000**, 1–3 (2017) Preprint 23 January 2017 Compiled using MNRAS LATEX style file v3.0

Investigating the Benefits of a Moveable Antenna Element for 21 cm Cosmology

Aaron Ewall-Wice,[1]★
[1]*MIT Kavli Institute for Astrophysics and Space Research, Cambridge, MA 02139*

Accepted XXX. Received YYY; in original form ZZZ

ABSTRACT
We investigate the efficacy of a moveable antenna to eliminate the wedge, a leading systematic limitation to 21 cm power spectrum experiments.

Key words: keyword1 – keyword2 – keyword3

1 INTRODUCTION

2 SIMULATIONS OF A SIMPLE ARRAY

I started by creating a simple simulation of 217 antennas in a hexagonal grid. Each antenna is assumed to be a circular aperture with a diameter of 2 meters and each antenna is spaced 3 meters apart. I computed the visibilities of these antennas for a single source with a flux of 1 Jy located at $m = 0$, $\ell = 0.9$. I compute visibilities with 100 kHz frequency resolution across a bandwidth of 20 MHz centered at 150 MHz. I than gridded the visibilities with the UV plane primary beam of a circular aperture given by (Vedantham & Koopmans 2015)

$$B_{uv}(x) = \begin{cases} \frac{2}{\pi}\left[\cos^{-1} x - x\sqrt{1-x^2}\right] & x \leq 1 \\ 0 & x > 1 \end{cases} \quad (1)$$

where $x = r/R_a$. The visibilities are gridded on the uv plane with a resolution of 0.5λ. The sampling function of the array is recorded on a separate uv plane by gridding visibilities equal to unity with the same gridding kernel as equation 1.

I compute the power spectrum in two ways.

(i) With a delay transform. Using the (Parsons et al. 2012) delay-transform, I take the 1d FFT of each visibility along the frequency direction with a Blackman-Harris window. After delay-transforming all visibilities, I bin and average cylindrically.

(ii) With a Fourier transform in the frequency direction of the gridded uv data. A Blackman-Harris window is also employed at the FT of each uv cell. The resulting (u, v, η) cube is than cylindrically averaged.

2.1 Results for a Hexagonal Configuration

We first investigate the fiducial hexagonal configuration. In Fig. 1 I show the image at 150 MHz of the point-source whose side-lobes (which are located at the center of the primary beam) dominate it significantly.

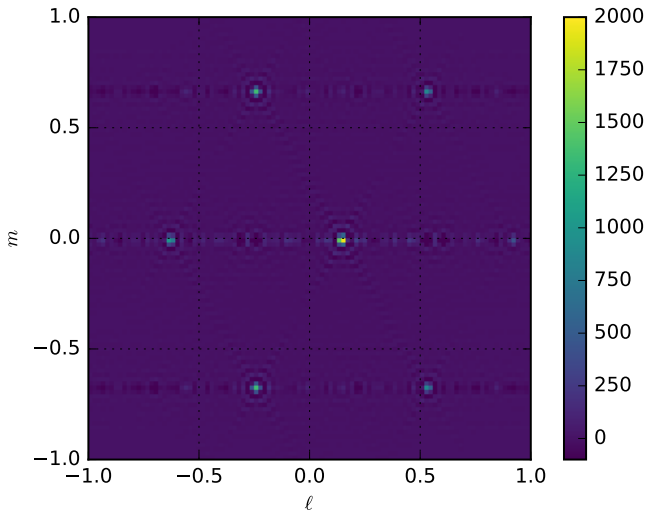

Figure 1. Image by a 217 antenna hexagonal array of a point source at $\ell = 0.9, m = 0$. The actual source is dwarfed by its side-lobe which is in the center of the primary beam.

In Fig. 2 I show the power spectrum of gridded visibilities compared to those obtained with the delay transform techniques. The level of foreground isolation required to measure the 21 cm signal is typically taken to be 10^{-5} so I plot the contour at which the foregrounds pass below 10^{-5} their peak value as a white-dashed contour. I plot the horizon wedge as a solid white line with a black-dashed line overlaid. We see that the foreground leakage from the gridded power spectrum vastly exceeds that in the delay-transform power spectrum. As is well known, redundant arrays are indeed abysmal for the imaging power-spectrum technique.

★ E-mail: aaronew@mit.edu

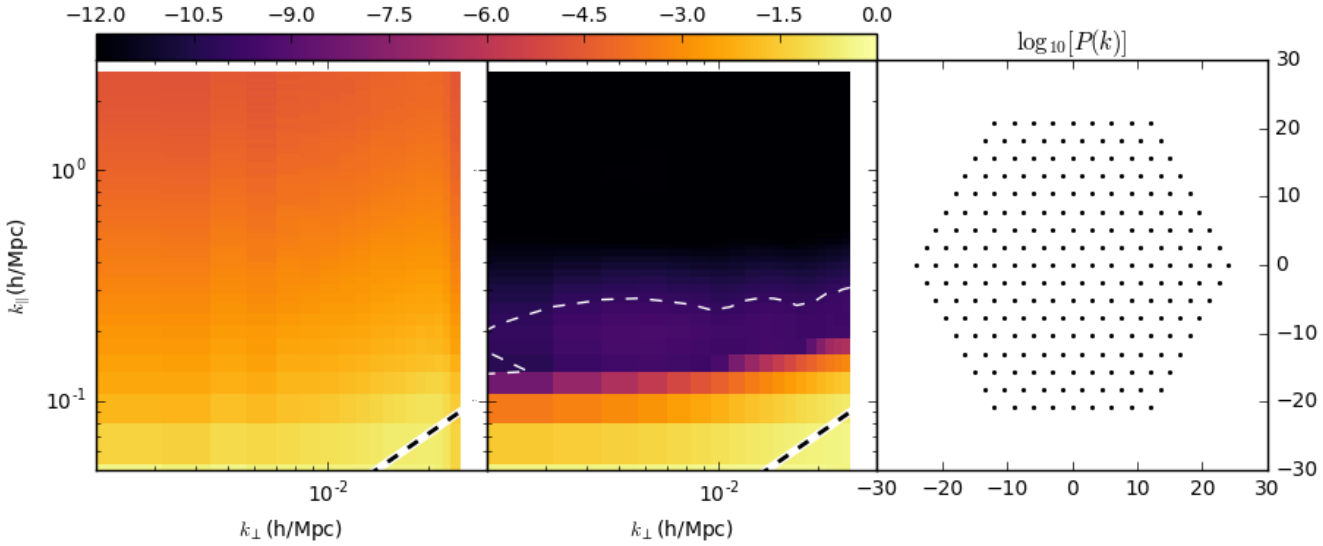

Figure 2. The cylindrical power spectrum for a 217 antenna hex array of 2 m apertures spaced by 3 m (Antenna positions are shown on the right). The horizon "Wedge" is drawn as a thick white line with a dashed black line overlayed. We demarcate the contour at which the power spectrum of the sources drops below 10^{-5} its maximum as a white dashed line. This level of isolation is typically assumed to be what is required for a detection of the 21 cm signal. Left: Power spectrum of gridded uv data with sampling function divided out. Right: The delay-transform power spectrum of the hex. We see that a hex has very poor imaging power-spectrum capabilities.

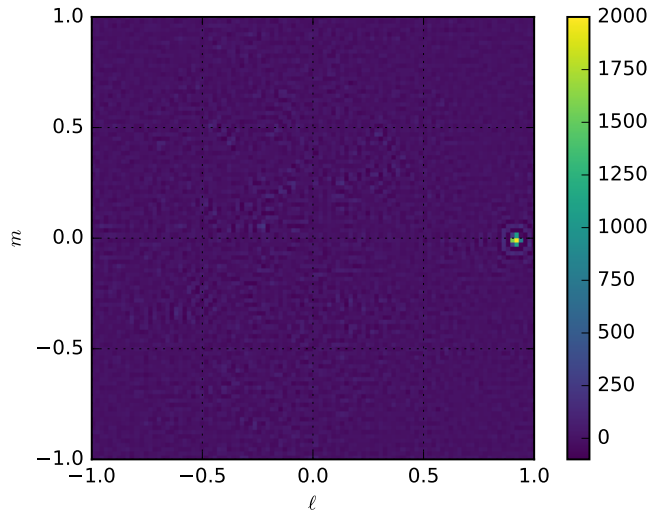

Figure 3. Image of a point source at $\ell = 0.9$, $m = 0$ by a 217 antenna hexagonal array of 2 m diameter apertures separated by 3 m with each position perturbed by $\sqrt{2} \times 3/2$ m. The side-lobes have been significantly suppressed relative to the hexagonal case.

2.2 Results for a Perturbed Hexes

Next, I perturb the locations of the hexagonally arranged antennas by $1/\sqrt{2}$ times their separations in a random direction. The resulting image at 150 MHz is shown in Fig. 3. We see that the side-lobes have been dramatically suppressed.

In Fig. 4 I show the delay and imaging power spectrum of the perturbed Hex. We see that foreground leakage is dramatically improved but the region of k-space accessible is still significanlty smaller than that accessible through the delay-spectrum technique.

2.3 Co-adding Many Perturbed Configurations

Next I try co-adding 10 and 100 different independent perturbed configurations before dividing out the sampling function and Fourier transforming. The image of an imaged source at with 10 co-added configurations is shown in Fig. 5. We inspect a power spectrum comparision in Fig. 6. While it is difficult to tell by simple inspection, some improvement has been achieved in the location of the 10^{-5} contour in the power spectrum (by $\approx 0.1h$/Mpc). This convergence is alarmingly slow and I'm hesitant to say that I'm actually doing this right (dividing out the correct sampling function). I repeat the experiment for 100 random configurations with the power spectrum showin in Fig. 7. To check that the gridded visibilities make sense, I show the gridded visibilities for various frequencies in Fig. 8.

I perform the same exercise for sources at $\ell = \{0.1, 0.25, 0.5, 0.0\}$. I show the resulting power spectra in Fig. 12.

The slow rate at which a single foregrounds contamination is mitigated through co-added integrations is somewhat discouraging. I will try looking at a filled aperture and than move to larger antennas with fewer elements (to reduce the primary beam width). One possibility is that large moveable antennas can be implemented in software by phased different sub-arrays over each night.

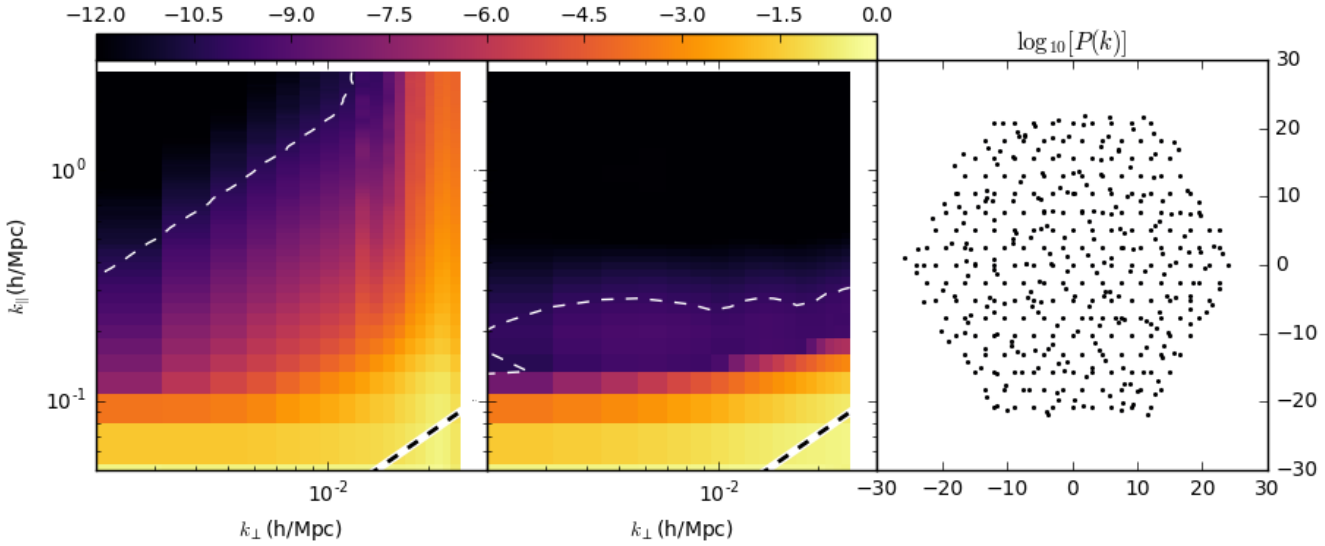

Figure 4. The cylindrical power spectrum for a 217 antenna hex array of 2 m apertures spaced by 3 m (Antenna positions are shown on the right). The horizon "Wedge" is drawn as a thick white line with a dashed black line overlayed. We demarcate the contour at which the power spectrum of the sources drops below 10^{-5} its maximum as a white dashed line. This level of isolation is typically assumed to be what is required for a detection of the 21 cm signal. Left: Power spectrum of gridded uv data with sampling function divided out. Right: The delay-transform power spectrum of the hex. We see that significant improvements in the imaging power spectrum ar obtained. However, contamination still extends beyond what exists for the delay-transform wedge.

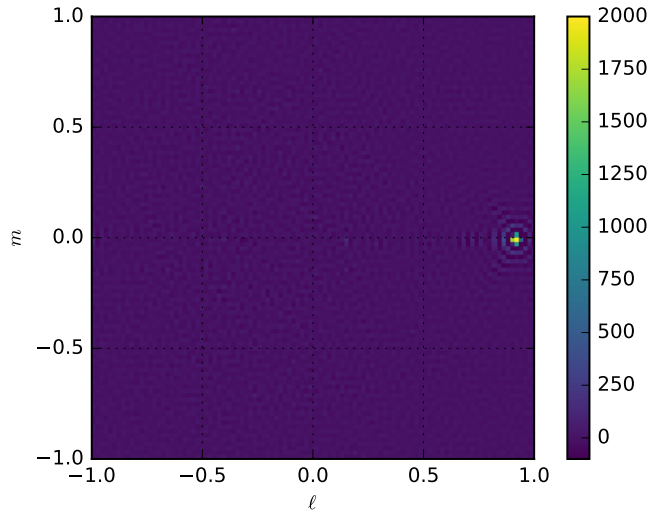

Figure 5. Image of a point source at $\ell = 0.9$, $m = 0$ by a 217 antenna hexagonal array of 2 m diameter apertures separated by 3 m with each position perturbed by $\sqrt{2}\times3/2$ m. Now the uv distribution has been integrated over 10 random perturbations to the Hex. The side-lobes have been significantly suppressed relative to the hexagonal case.

2.4 Multiple Sources

2.5 Filled Aperture Perturbed Hex

2.6 Large Antennas

REFERENCES

Parsons A. R., Pober J. C., Aguirre J. E., Carilli C. L., Jacobs D. C., Moore D. F., 2012, ApJ, 756, 165
Vedantham H. K., Koopmans L. V. E., 2015, MNRAS, 453, 925

This paper has been typeset from a TEX/LATEX file prepared by the author.

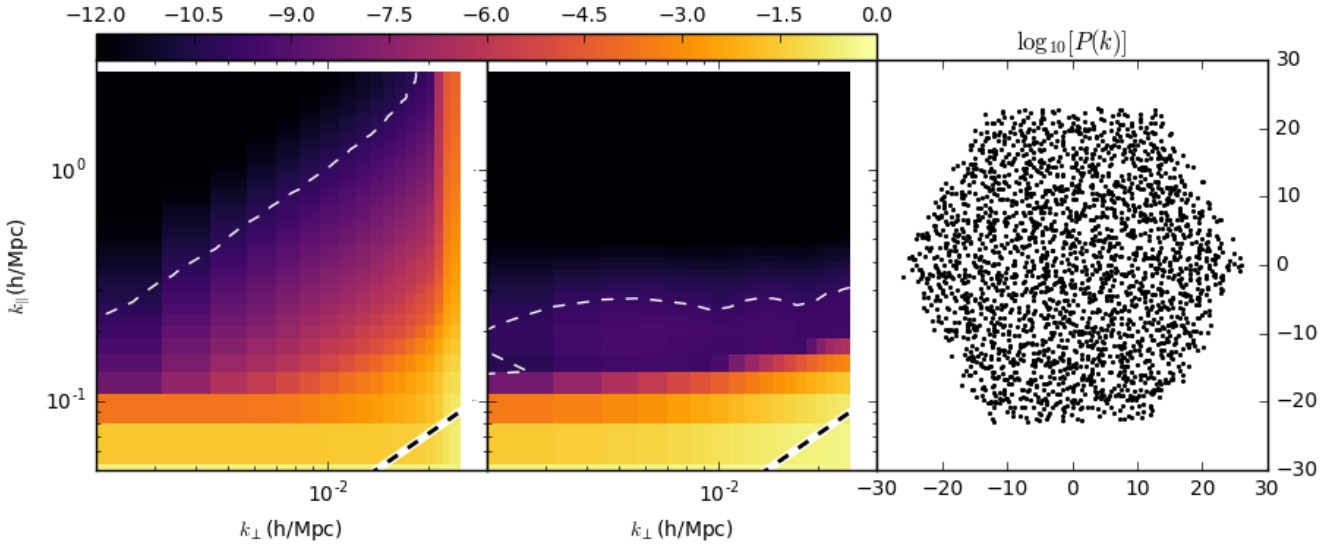

Figure 6. The cylindrical power spectrum for a 217 antenna hex array of 2 m apertures spaced by 3 m (Antenna positions are shown on the right). The antennas are perturbed in 10 different random configurations and the visibilities are co-added to the same uv plane. The horizon "Wedge" is drawn as a thick white line with a dashed black line overlayed. We demarcate the contour at which the power spectrum of the sources drops below 10^{-5} its maximum as a white dashed line. This level of isolation is typically assumed to be what is required for a detection of the 21 cm signal. Left: Power spectrum of gridded uv data with sampling function divided out. Middle: The delay-transform power spectrum of the hex. We see that significant improvements in the imaging power spectrum ar obtained. However, contamination still extends beyond what exists for the delay-transform wedge. Right: Co-added antenna positions.

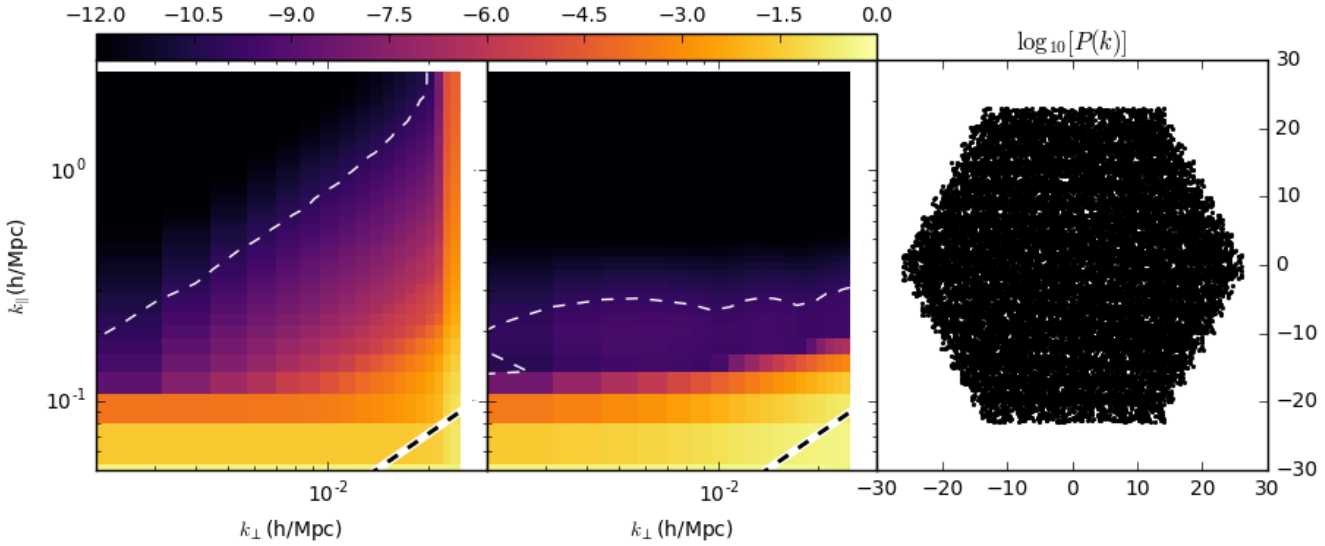

Figure 7. The cylindrical power spectrum for a 217 antenna hex array of 2 m apertures spaced by 3 m (Antenna positions are shown on the right). The antennas are perturbed in 100 different random configurations and the visibilities are co-added to the same uv plane. The horizon "Wedge" is drawn as a thick white line with a dashed black line overlayed. We demarcate the contour at which the power spectrum of the sources drops below 10^{-5} its maximum as a white dashed line. This level of isolation is typically assumed to be what is required for a detection of the 21 cm signal. Left: Power spectrum of gridded uv data with sampling function divided out. Middle: The delay-transform power spectrum of the hex. We see that significant improvements in the imaging power spectrum ar obtained. However, contamination still extends beyond what exists for the delay-transform wedge. Right: Co-added Antenna positions.

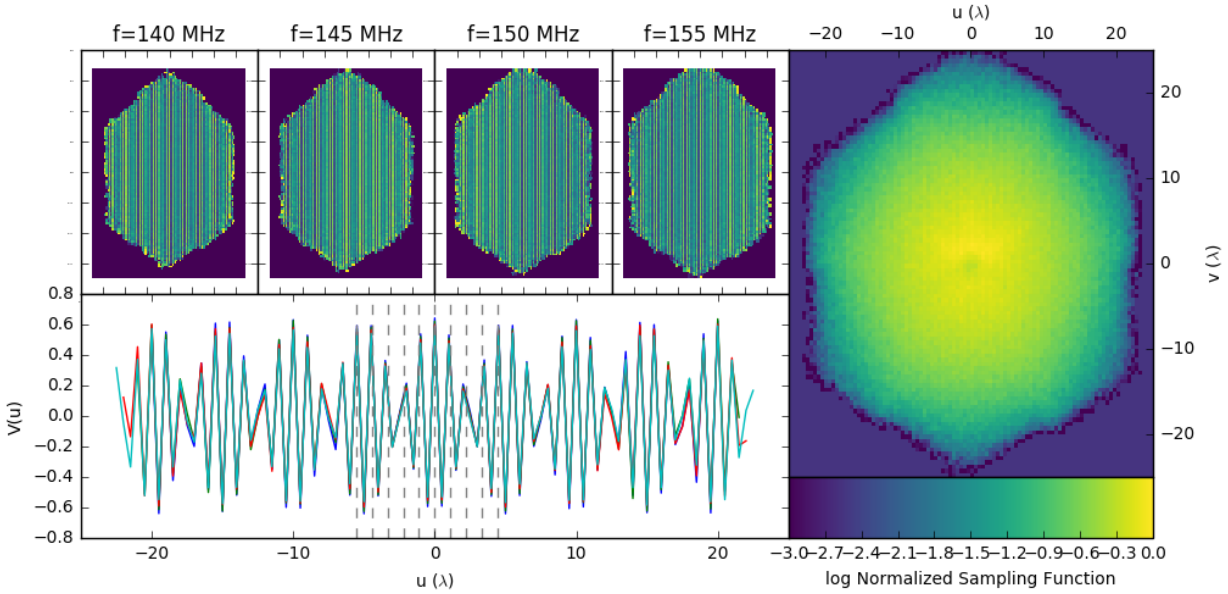

Figure 8. Top Left: the real component of the uniformly-weighted gridded visibilities for our off axis ($\ell = 0.9$ source for several different frequency slices. Bottom: The average of the four slices along the $v - axis$ (where the sampling function was not zero). Right: The logarithm of the array sampling function, noramalized to unity. Some aliasing is visible on the bottom left plot due to the finite dish size. Vertical dashed lines indicate the expected locations of the fringe peaks.

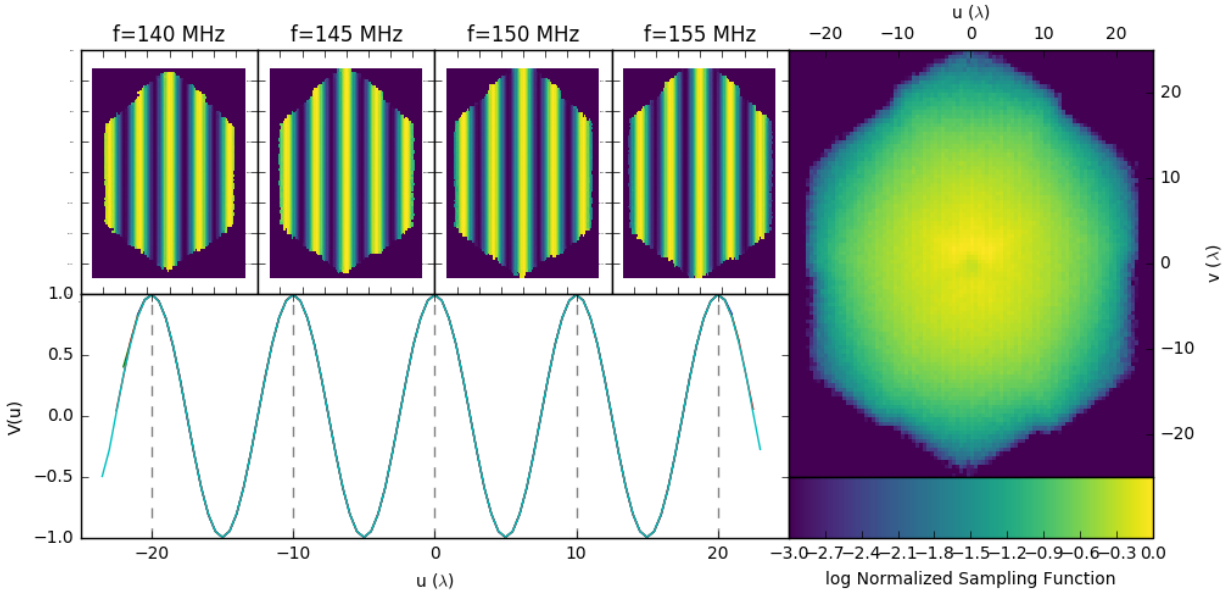

Figure 9. Same as Fig. 8 but for a source with $\ell = 0.1$.

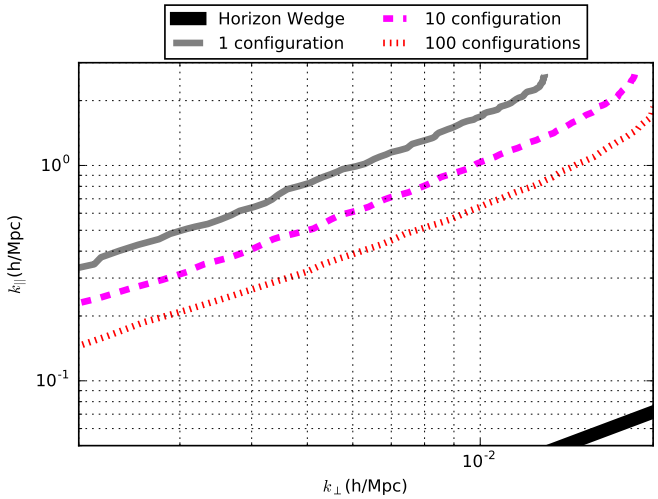

Figure 10. Lines in cylindrical k-space in which the foreground level goes below 10^{-5} its peak. Increasing the number of co-added integrations appears to monotonically improve the degree of foreground isolation but in all cases up to 100 co-added integrations, the contamination significantly exceeds the level.

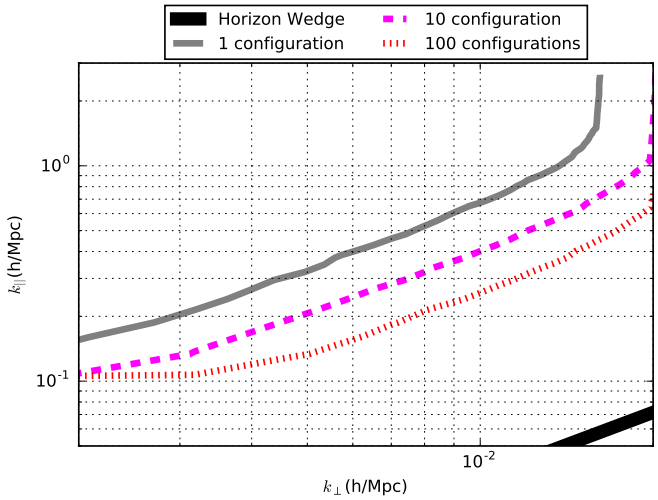

Figure 11. Same as Fig. 10 but for a single source with $\ell = 0.1$ instead of $\ell = 0.9$.

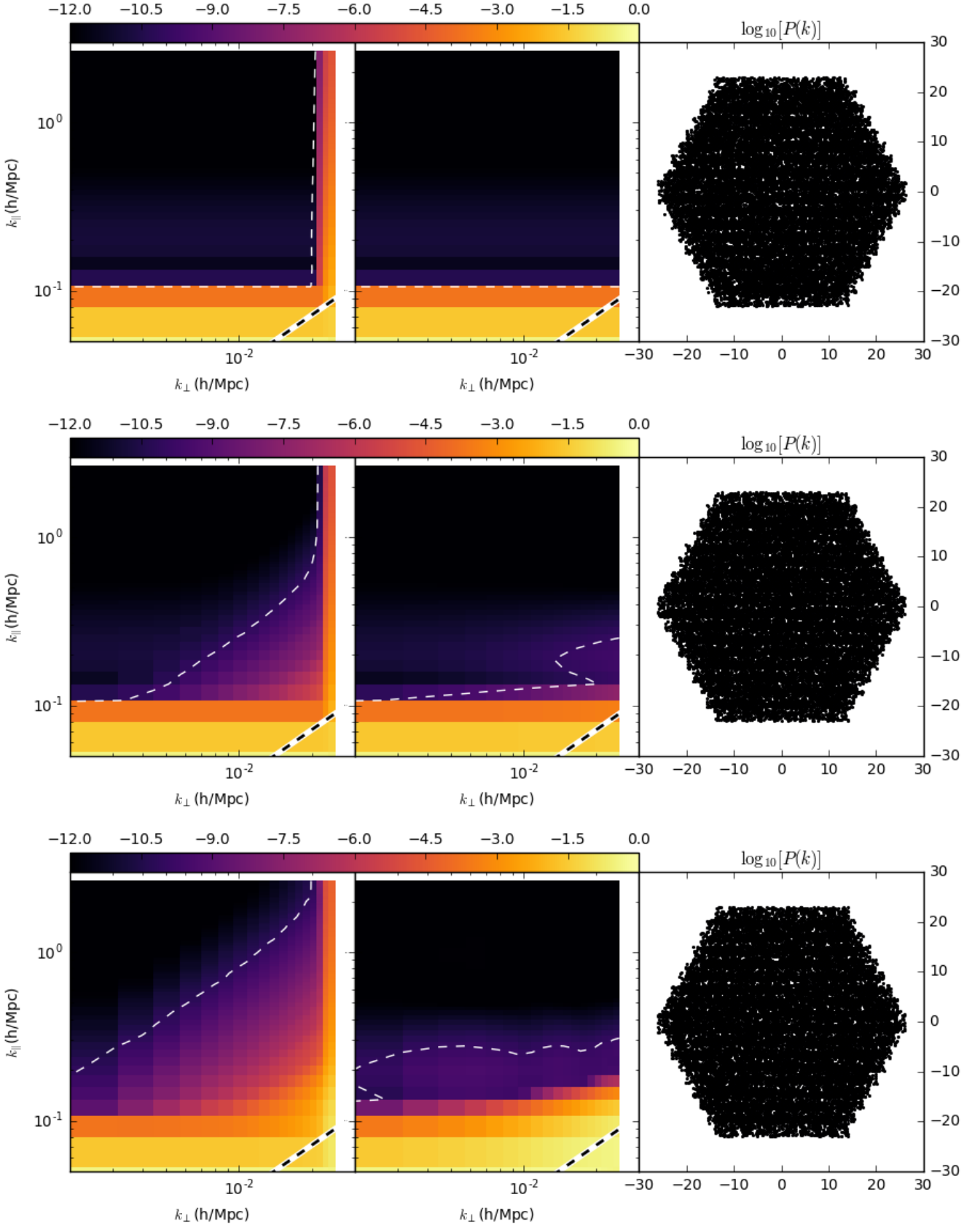

Figure 12. Power Spectra for 100 co-added antenna configurations with 2 m apertures spaced 3 m apart and perturbed $3 \times \sqrt{2}/2$ m for sources at $\ell = 0$(top), $\ell = 0.1$ (middle) and $\ell = 0.9$ (bottom). We see that a zenith sourch in both the imaging and visibility power spectrum is centered at $k_\parallel = 0$ with no leakage. A source that is only six degrees off zenith imposes significant leakage in the imaging power spectrum.